Detecting entrainment in Fermi-Bose mixtures

Khalid Hossain [1,*] Subhadeep Gupta,[2,†] and Michael McNeil Forbes [1,2,‡]

[1]*Department of Physics and Astronomy, Washington State University, Pullman, Washington 99164-2814, USA*
[2]*Department of Physics, University of Washington, Seattle, Washington 98195-1560, USA*

We propose an experimental protocol to directly detect the Andreev-Bashkin effect (entrainment) in the bulk mixture of a bosonic and fermionic superfluid using a ring geometry. Our protocol involves the interferometric detection of the entrainment-induced phase gradient across a superfluid due to the flow of another in which it is immersed. The choice of ring geometry eliminates variations in the stronger mean-field interaction which can thwart the detection of entrainment in other geometries. A significant enhancement of the entrainment phase-shift signal is possible, if the dimer-boson scattering length turns out to be large, which can be measured by tuning the interaction to the limit of miscibility of the two superfluids. With suggested improvements and careful design implementation, one may achieve approximately 67% shift in the interferometer fringes.

I. INTRODUCTION

Superfluid entrainment plays a crucial role in the dynamics of superfluid mixtures in neutron stars. The effect, whereby a flowing superfluid drags along or "entrains" another superfluid despite the lack of dissipation, was first predicted by Andreev and Bashkin for mixtures of superfluid ^{3}He and ^{4}He [1,2]. Since its prediction, superfluid entrainment has been studied extensively in the contexts of neutron stars, nuclear physics [3–7], and cold atoms [8–16], but despite almost half a century of study, it has yet to be directly observed in experiments.

Cold-atom systems provide a new environment in which to search for entrainment where one has exquisite control over both geometry and interactions [17]. Entrainment manifests as an effective potential for one superfluid species induced by the flow of another. This property can be used to induce a phase winding, which can then be measured using interferometry. In this paper we outline a procedure using this effect to directly observe entrainment in a two-species mixture of superfluid ^{6}Li and ^{174}Yb, taking advantage of the large mass of the bosons and the availability of species-specific potentials.

On a nuclear scale, neutron stars are cold and the crust is expected to comprise a mixture of superfluid neutrons and superconducting protons [18]. These superfluids act as an internal reservoir of angular momentum, which may be suddenly transferred to the crust through vortex (un)pinning or hydrodynamic instabilities, resulting in a sudden increase in the rotation rate of the stars, observed as a "glitch" in pulsar data [19–38]. Although the detailed mechanism behind glitches remains a mystery, it is clear that superfluid dynamics and entrainment between the proton and neutron fluids play a

significant role [39] owing to the strength of the nuclear interactions. Unfortunately, being light years away, astrophysical bodies like neutron stars and pulsars are extremely difficult to measure.

For this reason we turn to ultracold-atom experiments, where one can create superfluid mixtures [40–42] to act as quantum simulators of neutron-star physics [43,44]. The challenge with terrestrial experiments is that the magnitude of the entrainment effect depends on the interspecies interaction strength g_{ab}, which must generally be small $g_{ab}^2 < g_{aa}g_{bb}$ to allow the superfluids to mix. This frustrates detection in ^{3}He and ^{4}He superfluid mixtures [45], where the mutual interactions require temperatures below that which can be achieved by state-of-the-art cryogenics in order for the fluids to not phase separate [46,47]. In dilute Bose gases, the entrainment is further suppressed as it occurs at second order, depending on the square of the interspecies interactions [12,48]. This thwarts attempts to measure the entrainment through, for example, modifications of the dipole frequency [49] because mean-field effects dominate. For the ^{174}Yb -^{6}Li superfluid mixture considered here, the calculated value of the dipole frequency shift due to entrainment is approximately equal to only 0.02%, two orders of magnitude smaller than the observed shift [42] from mean-field effects.

In addition to serving as a suitable system to observe entrainment, a mixture of fermionic and bosonic superfluids also serves as a versatile platform for other studies in many-body physics. The Fulde-Ferrell-Larkin-Ovchinnikov phase [50–52], time-reversal-invariant superfluids with exotic topological properties [53], rotational responses [54], and the dynamics and structure of solitons [55] can be explored by tuning the mass ratios, particle densities, and interparticle interactions. Interesting physical properties such as the ground-state characteristics of a mixture [56], quasiparticle excitation spectrum [57], general phase diagram [58], phase competition among density wave orderings and superfluid pairings [59], and many-body effects in the mixture [60]

*mdkhalid.hossain@wsu.edu
†deepg@uw.edu
‡mforbes@alum.mit.edu

have been explored in great detail in the presence of optical lattice potentials, facilitating the interplay between nonlinearity and periodicity. Entrainment, in particular, has been investigated theoretically for two-component [61–64] and multicomponent [65] Bose-Bose mixtures in optical lattices. By introducing an optical lattice to the superfluid mixture, one may enhance the entrainment signal by softening the phonon dispersion relationship [62].

A mixture of superfluid ^{6}Li and ^{174}Yb provides a favorable environment in which to detect entrainment. The ^{6}Li scattering length may be tuned with a Feshbach resonance [66], allowing us to amplify entrainment effects while ensuring that the fermionic ^{6}Li superfluid remains mixed with the bosonic superfluid ^{174}Yb. As mentioned above, although dipole oscillations provide a natural place to search for entrainment, mean-field effects dominate the frequency shift in cold-atom systems. We will use these mean-field effects to test our microscopic theory, but then carefully design a procedure to eliminate these mean-field effects by placing the two components in ring traps. Our proposal is similar to that suggested in [48] but differs in details for removing mean-field contamination and in using interferometry to measure the effective entrainment. Another idea proposed in [8] is to enhance entrainment with tight confinement to induce a dimensional reduction. In contrast, with the enhancements discussed in this paper, we expect to be able to directly observe bulk entrainment in three dimensions.

We propose to use a common optical ring to trap miscible fermionic and bosonic superfluids in the same region of space and then to generate a relative flow between them by inducing a persistent current in the fermionic superfluid while using a species-selective optical barrier to prevent the bosonic superfluid from flowing. The effect of entrainment is to induce a phase gradient in the bosonic superfluid even though flow is prevented with the barrier. This gradient will be observed as a phase shift in the matter-wave interference pattern generated as follows. After equilibration, the fermions are removed with a rapid resonant laser pulse to minimize mean-field effects. The bosons are then released by switching off all the potentials, allowing them to expand and interfere across the previous site of the barrier. Entrainment can then be measured by correlating the phase shift of the interference pattern with the magnitude and direction of the flow in the fermionic superfluid.

The rest of the paper is organized as follows. In Sec. II we derive the mean-field equations of motion for the mixture with entrainment interaction. Section III discusses the proposed experiment. In Sec. IV we estimate the phase shift. The main results and a detailed discussion of the physics of the detection are presented in Sec. V: suitable experimental parameters in Sec. V A and characteristics of the detectable signal in Sec. V B. We summarize in Sec. VI.

II. THEORY

First we consider a dilute single-component bosonic superfluid at $T = 0$. If the interactions are weak, we may describe this in the mean-field approximation by the usual Gross-Pitaevskii equation (GPE) for the condensate wave function ψ_b. This is related through a Madelung transform to the super-

fluid density $n(\mathbf{r}, t)$ and phase velocity $\mathbf{v} = \frac{\hbar}{m} \nabla \phi$, where ϕ is the momentum potential and $\psi_b = \sqrt{n_b} e^{i\phi}$. The GPE follows from the Lagrangian density

$$\mathcal{L}[\psi_b] = i\hbar \psi_b^\dagger \dot{\psi}_b - \mathcal{E}(\psi_b), \tag{1a}$$

$$\mathcal{E}(\psi_b) = \frac{\hbar^2 \nabla \psi_b^\dagger \cdot \nabla \psi_b}{2m_b} + \overbrace{\frac{g_{bb}}{2}(\psi_b^\dagger \psi_b)^2}^{\mathcal{E}_b(n_b)}, \tag{1b}$$

where $g_{bb} = 4\pi\hbar^2 a_{bb}/m_b$ is the coupling constant, a_{bb} is the s-wave scattering length between the bosons, and m_b is the mass of the bosons. The equations of motion give rise to the usual GPE

$$i\hbar \dot{\psi}_b(\mathbf{r}, t) = -\frac{\hbar^2 \nabla^2}{2m_b} \psi_b(\mathbf{r}, t) + \overbrace{g_{bb} n_b(\mathbf{r}, t)}^{\mathcal{E}_b'(n_b)} \psi_b(\mathbf{r}, t). \tag{2}$$

This formulation describes the dynamics of a weakly interacting Bose-Einstein condensate (BEC) where the equation of state for homogeneous matter is $\mathcal{E}_b(n_b) = g_{bb} n_b^2/2$.

However, the same formulation can be modified to describe the BEC limit of the BCS-BEC crossover of symmetric (unpolarized) fermionic superfluids with resonant s-wave interactions (see [67] for a review). In this limit, the fermionic superfluid can be modeled with a similar equation, known as an extended Thomas-Fermi (ETF) model, which describes the fermionic superfluid as a gas of condensed bosonic dimers with number density $n_D = n_f/2$. The ETF model for this system is similar to the GPE with three modifications: (i) the mass is replaced by the dimer mass $m_D = 2m_f$, where m_f is the mass of the fermionic components (^{6}Li in our case), (ii) the density $n_D = \psi_D^\dagger \psi_D = n_f/2$ is interpreted as the dimer density rather than the fermion density, and (iii) the interaction is replaced by the homogeneous equation of state in the crossover $\mathcal{E}_f(n_f)$ that depends on the magnetic field B through the fermion-fermion scattering length $a_{ff}(B)$:

$$i\hbar \dot{\psi}_D(\mathbf{r}, t) = -\frac{\hbar^2 \nabla^2}{2m_D} \psi_D(\mathbf{r}, t) + \frac{\partial \mathcal{E}_f(2n_D)}{\partial n_D} \psi_D(\mathbf{r}, t). \tag{3}$$

Well justified in the BEC limit, this formulation continues to work quite well in the unitary limit where $a_{ff} \to \infty$, where it correctly describes [68] the hydrodynamics of rather violent collisions [69] and qualitative properties of vortex dynamics [70]. Some of this success comes from the fact that this ETF model correctly reproduces the low-lying phonon spectrum

$$E_{\mathrm{ph}}(\hbar k) = \sqrt{\frac{\hbar^2 k^2}{4m_f} \left(\frac{\hbar^2 k^2}{4m_f} + 4\mathcal{E}_f''(n_f) n_f \right)}, \quad k \ll k_F, \tag{4}$$

where $4\mathcal{E}_f''(n_f) = \partial^2 \mathcal{E}_f(2n_D)/\partial n_D^2$, although it fails to predict pair breaking and associated phenomena which occur near $k \sim k_F$. This correctly reproduces the speed of sound c_s where $E_{\mathrm{ph}}(\hbar k) \sim \hbar k c_s$ is linear in both the BEC and the unitary Fermi gas (UFG) limits

$$c_s^2 = \frac{g_{DD} n_D}{m_D}, \quad \mathcal{E}_f \sim \frac{-\hbar^2 n_f}{2m_f a_{ff}^2} + \frac{g_{DD} n_D^2}{2}\bigg|_{a_{ff} \ll 1}, \tag{5a}$$

$$c_s^2 = \frac{\xi}{3} v_f^2, \quad \mathcal{E}_f \sim \xi \frac{\hbar^2 (3\pi^2 n_f)^{5/3}}{10\pi^2 m_f}\bigg|_{a_{ff} \to \infty}, \tag{5b}$$

respectively, where $g_{DD} \approx 0.6a_{ff}$ is the dimer-dimer scattering length [71] and $\xi = 0.3742(5)$ [72] is the universal Bertsch parameter [73] (see also [74,75]), combining experiment [76,77] and quantum Monte Carlo (QMC) [78,79] values. In our analysis, we use a Padé approximant for $\mathcal{E}_f(n_f)$ that correctly interpolates between the unitary and BEC limits including QMC values for the Tan contact [80,81] and few-body parameters in the deep BEC limit [82,83].

The Lagrangian (1a) is Galilean invariant under a boost of velocity $\boldsymbol{v}$ with an appropriate phase redefinition

$$\psi(\boldsymbol{x}, t) \to e^{i\phi}\psi(\boldsymbol{x} - \boldsymbol{v}t, t), \quad \hbar\phi = m\boldsymbol{v} \cdot \boldsymbol{x} - \frac{mv^2 t}{2}. \quad (6)$$

The generalization for two components, a boson ψ_b and a dimer ψ_D, has a similar form, but admits other terms allowed by Galilean covariance. For the weakly interacting case, we add a term coupling the phase gradients of the two components:

$$\psi_{D,b} = \sqrt{n_{D,b}}\,e^{i\phi_{D,b}}, \quad m_{D,b}\boldsymbol{v}_{D,b} = \hbar\nabla\phi_{D,b}, \quad (7a)$$

$$\mathcal{L} = i\hbar(\psi_D^\dagger \dot{\psi}_D + \psi_b^\dagger \dot{\psi}_b) - \mathcal{E}[\psi_D, \psi_b, \nabla\psi_D, \nabla\psi_b], \quad (7b)$$

$$\mathcal{E}[\psi_D, \psi_b] = \frac{\hbar^2}{2m_D}|\nabla\psi_D|^2 + \frac{\hbar^2}{2m_b}|\nabla\psi_b|^2$$
$$- \underbrace{\rho_{\mathrm{dr}}(n_D, n_b)|\boldsymbol{v}_D - \boldsymbol{v}_b|^2}_{\mathcal{E}_{\mathrm{ent}}}$$
$$+ \underbrace{g_{bb}\frac{n_b^2}{2} + g_{Db}n_D n_b + \mathcal{E}_f(2n_D)}_{\mathcal{E}_h(n_D, n_b)},$$

$$g_{bb} = \frac{4\pi\hbar^2 a_{bb}}{m_b}, \quad g_{Db} = \frac{2\pi\hbar^2 a_{Db}(m_D + m_b)}{m_D m_b}. \quad (7c)$$

Here ρ_{dr} has the dimension of mass density, as in $\rho = mn$. In addition, $\mathcal{E}_{\mathrm{ent}}$ is the entrainment term:

$$|\boldsymbol{v}_D - \boldsymbol{v}_b|^2 = \frac{\hbar^2}{m_D n_D m_b n_b}\left|\sqrt{\frac{m_b}{m_D}}\psi_b\nabla\psi_D - \sqrt{\frac{m_D}{m_b}}\psi_D\nabla\psi_b\right|^2.$$

This term is manifestly Galilean invariant since it contains a difference between what is sometimes called the superfluid velocities $\boldsymbol{v}_i = \hbar\nabla\phi_i/m_i$. Note that, for simple superfluids with only a single quadratic gradient term $|\nabla\psi|^2$, this superfluid velocity corresponds to the group velocity $\boldsymbol{j}_i/m_i n_i$, but the presence of additional gradient terms, such as this entrainment term, changes the relationship between the phase gradients $\nabla\phi$ and the group velocity. In particular, as we will see, entrainment allows a phase gradient to appear in a system even in the absence of a current, providing a way detect entrainment through interference.

Miscibility of the bosonic and fermionic superfluids, i.e., that they occupy the same physical space, is a requirement for detecting entrainment. A necessary condition for miscibility is that the energy density be convex:

$$\left(\frac{\partial^2\mathcal{E}_h}{\partial n_D\partial n_b}\right)^2 < \frac{\partial^2\mathcal{E}_h}{\partial n_D^2}\frac{\partial^2\mathcal{E}_h}{\partial n_b^2} \Rightarrow \frac{\pi\hbar^2(1 + \frac{m_b}{m_D})^2}{4m_b a_{bb}} < \frac{\mathcal{E}_f''(n_f)}{a_{Db}^2}. \quad (8)$$
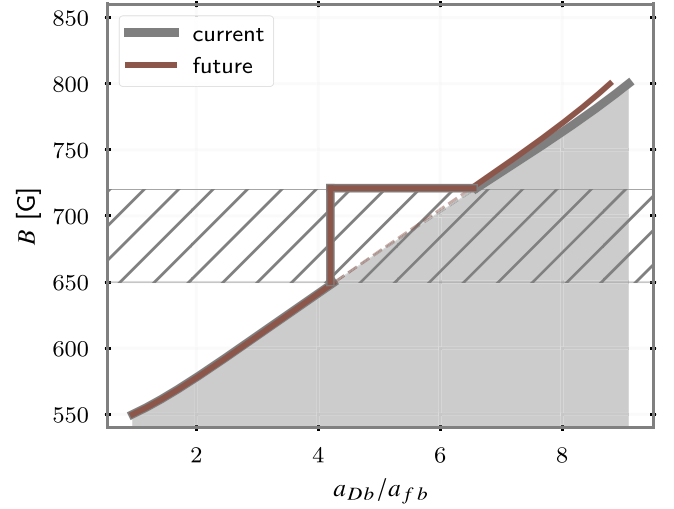

FIG. 1. Miscibility condition (8) as a function of a_{Db}/a_{fb} [87] and magnetic field B. The shaded region corresponds to immiscible fluids which cannot be used to measure entrainment. To maximize the entrainment signal, one should generally choose the smallest magnetic field allowed by the miscibility condition (solid lines). Within the hatched region, however, particle losses are particularly high [88]. Thus if $4 \lesssim a_{Db}/a_{fb} \lesssim 6.5$, one should keep $B \approx 730$ G to maintain a reasonable lifetime of the system.

For our setup, the quantities on the left-hand side are fixed, but the right-hand side can be adjusted using the Li resonance through the B-field dependence of $\mathcal{E}_f(n_f)$ to ensure that our mixture remains miscible as we attempt to maximize the entrainment.

In particular, the miscibility depends sensitively on the dimer-boson scattering length a_{Db}. Naively, one might expect this to be twice the Fermi-Bose scattering length $a_{Db} \sim 2a_{fb}$, but mean-field effects enhance this $a_{Db} \sim 3.87a_{fb}$ for our $m_{\mathrm{Yb}}/m_{\mathrm{Li}} \approx 29$ mass ratio [84–86]. However, as pointed out in [84], a_{Db} may receive large in-medium corrections from three-body effects, which must be calibrated to the system under consideration. We thus consider a_{Db}/a_{fb} as an unknown parameter which must be carefully measured and present our main results for a range of plausible values (see Fig. 1).

The resulting energy-density functional can be cast in terms of a wave-function-dependent effective mass matrix for the two-component wave function $\boldsymbol{\Psi} = (\psi_D, \psi_b)^T$:

$$\mathcal{E}[\boldsymbol{\Psi}] = \frac{\hbar^2}{2}\nabla\boldsymbol{\Psi}^\dagger \cdot \boldsymbol{M}^{-1} \cdot \nabla\boldsymbol{\Psi} + \mathcal{E}_h, \quad (9a)$$

$$\boldsymbol{M}^{-1}[\psi_D, \psi_b] = \begin{pmatrix} m_D^{-1} - f_{\mathrm{ent}}\frac{m_b}{m_D}n_b & f_{\mathrm{ent}}\psi_b^\dagger\psi_D \\ f_{\mathrm{ent}}\psi_D^\dagger\psi_b & m_b^{-1} - f_{\mathrm{ent}}\frac{m_D}{m_b}n_D \end{pmatrix}, \quad (9b)$$

where

$$f_{\mathrm{ent}}(n_D, n_b) = \frac{\rho_{\mathrm{dr}}}{m_D m_b n_D n_b}. \quad (9c)$$

Varying the associated action with respect to $\boldsymbol{\Psi}^\dagger$ gives the coupled nonlinear Schrödinger equations

$$i\hbar e^{i\eta}\dot{\boldsymbol{\Psi}} = -\frac{\hbar^2}{2}\nabla(\boldsymbol{M}^{-1}[\psi_{D,b}] \cdot \nabla\boldsymbol{\Psi}) + \boldsymbol{V}_{\mathrm{eff}}[\psi_{D,b}] \cdot \boldsymbol{\Psi}. \quad (10)$$

Here we include a complex phase η to simulate thermal dissipation [sometimes referred to as the dissipative GPE (DGPE) or projected DGPE] and the effective potential is

$$V_{\text{eff}} = \begin{pmatrix} \frac{\partial \mathcal{E}_h}{\partial n_D} & 0 \\ 0 & \frac{\partial \mathcal{E}_h}{\partial n_b} \end{pmatrix} + \alpha \frac{\hbar^2}{2} \begin{pmatrix} \frac{\partial f_{\text{ent}}}{\partial n_D} & 0 \\ 0 & \frac{\partial f_{\text{ent}}}{\partial n_b} \end{pmatrix}$$
$$- f_{\text{ent}} \frac{\hbar^2}{2} \begin{pmatrix} \frac{m_D}{m_b}|\boldsymbol{\nabla}\psi_b|^2 & -\boldsymbol{\nabla}\psi_b^\dagger \cdot \boldsymbol{\nabla}\psi_D \\ -\boldsymbol{\nabla}\psi_D^\dagger \cdot \boldsymbol{\nabla}\psi_b & \frac{m_b}{m_D}|\boldsymbol{\nabla}\psi_D|^2 \end{pmatrix},$$
$$\alpha = -\frac{m_b}{m_D} n_b |\boldsymbol{\nabla}\psi_D|^2 - \frac{m_D}{m_b} n_D |\boldsymbol{\nabla}\psi_b|^2$$
$$+ \psi_D^\dagger \psi_b \boldsymbol{\nabla}\psi_b^\dagger \cdot \boldsymbol{\nabla}\psi_D + \psi_b^\dagger \psi_D \boldsymbol{\nabla}\psi_D^\dagger \cdot \boldsymbol{\nabla}\psi_b.$$

For weakly interacting bosons, $\mathcal{E}_f(2n_D) \equiv g_{DD} n_D^2/2$, Shevchenko and Fil [48] calculated ρ_{dr} to leading order in the interspecies coupling g_{Db} in terms of the phonon dispersion relationships $E_{\text{ph}}(\hbar k)$. We apply their results to our Bose-Fermi mixture by using (4) for the dimers instead of the usual bosonic phonon dispersion. The resulting expressions are rather complicated to display analytically, so we include a simple numerical implementation in Refs. [89,90]. This approach captures the correct physics in the deep BEC limit of the crossover where $E_{\text{ph}}(\hbar k)$ approaches the usual bosonic dispersion for the dimers and provides a qualitative extrapolation to the unitary regime.

To more accurately characterize the unitary regime, a fermionic density functional theory such as the superfluid local density approximation [91] should be used. In particular, our approximation neglects the softening of the phonon dispersion relationship and pair-breaking effects. We expect this to provide an upper bound on the magnitude of the entrainment since softening the dispersion *increases* the number of virtual excitations that contribute to entrainment. A similar enhancement can be achieved by using an optical lattice to modify the dispersion, as discussed in [62].

Another limit of our approach is the inclusion of only s-wave interactions at $T = 0$. This is appropriate in ultracold dilute gases, but may need corrections at finite temperature or if the density becomes large enough that Lee-Huang-Yang corrections become significant [92]. These corrections can easily be incorporated in a similar formalism, but require more thorough *ab initio* calculations or measurements to determine the exact form of the nonlinear interactions.

III. PROPOSED EXPERIMENT

Using this formalism, we model a mixture of a fermionic (^{6}Li, $^2S_{1/2}$) superfluid and a bosonic (^{174}Yb, $^1S_0$) superfluid. Using the wide s-wave Feshbach resonance centered at 832 G, one can tune the fermionic a_{ff} scattering length between the two lowest hyperfine states of Li [66,93]. Since Yb is not magnetically susceptible, the a_{bb} scattering length is fixed.

We propose using an optical ring trap to hold both superfluids with the ring oriented horizontally. Several convenient values for wavelength exist above 700 nm, although the polarizabilities of the two species will be different (for instance, at a wavelength of 780 nm the polarizability ratio of Li to Yb is about 5), the minima of the potentials coincide, trapping clouds in the same region of space but with different trapping
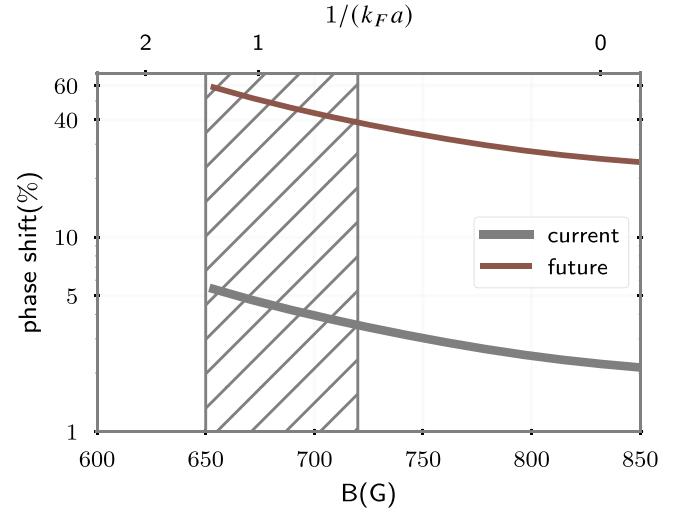

FIG. 2. Magnetic-field dependence of the phase shift for the mean-field value of $a_{Db} = 3.87 a_{fb}$. The unitary Fermi gas is realized at the resonance $B = 832$ G, where $k_F a_{\text{Li}} = \infty$. Here we show an example calculation performed for both current and future parameters as listed in Table I. The hatched region is the range within which the particle losses become significantly higher.

frequencies. In the vertical direction, the weaker gravitational force on the Li can be countered with a magnetic-field gradient to ensure physical overlap of the superfluids [94].

A circular flow around the ring will then be generated in the fermionic superfluid, for example, by using the procedure of optical stirring [95] with a laser beam which acts as a species-selective potential for Li. A convenient wavelength is 665 nm, where the polarizability ratio is about 60. Such techniques can generate circular flow with four windings, corresponding to a flow velocity $v/v_c \approx 0.1$ [95], where v_c is the local speed of sound in the center of the cloud. We use this as a lower bound in our estimates below.

While phase imprinting using a two-photon Raman transition between hyperfine states [96,97] is an alternative procedure to generate circulation states in BECs, it is not possible to adapt this to s-wave paired fermionic superfluids because the pairs are composed of two different hyperfine states. It may be possible to apply phase imprinting using an optical pulse with a tailored intensity profile as proposed in [98]. For optimization of the final experiment, the key is to maximize the flow in the fermions, while maintaining superfluidity, and minimizing the disturbance of the bosonic component.

As discussed below, the entrainment signal is maximized at lower magnetic fields (BEC limit) where the fermionic superfluid density increases. This can however cause two undesirable effects: the immiscibility of the fluids and increased three-body loss. To mitigate these issues, we propose generating the flow at $B = 832$ G UFG resonance and then slowly reducing B to maximize the signal once the flow is established (see Fig. 2). The loss of miscibility at low B has the interesting side effect of allowing one to estimate the value of a_{Db} by tuning the magnetic field to the limit of miscibility.

To prevent flow in the bosonic superfluid, a species-selective repulsive barrier seen only by the bosons can be

TABLE I. Parameters ranging from current to future values and the corresponding phase shifts.

Adjustable parameters	Fixed parameters
N_f: 10^5–10^6	$m_f = 6$ u
N_b: 10^5–10^6	$m_b = 174$ u
B: miscibility limited	$\omega_{\mathrm{Yb}} = 2\pi \times 400$ Hz
R: 30–200 μm	$a_{bb} = 5.5$ nm
	$a_{fb} = 1.59$ nm
	$\alpha = 6.2$
v/v_c: 0.15–0.2	$\xi = 0.3705$
$\Delta\theta/2\pi$: 3%–33% (+ in Fig. 3)	$a_{Db} = 2a_{fb}$, 578 G
$\Delta\theta/2\pi$: 6%–67% (× in Fig. 3)	$a_{Db} = 3.87a_{fb}$, 638 G

inserted. A convenient optical frequency for this potential is about 200 GHz blue detuned of the $^1S_0 \to {}^3P_1$ transition at 556 nm for Yb. After letting the two superfluids equilibrate, the bosonic superfluid will acquire a phase difference across the barrier due to the entrainment terms. This can subsequently be measured by observing the interference pattern after expansion [99].

This might seem unusual since the barrier arrests any flow in the bosonic superfluid $\boldsymbol{v}_b = 0$, so how can a phase shift accumulate? The resolution is that entrainment modifies the relationship between the phase gradient $\nabla\phi_{b/D}$ and the group velocity $\boldsymbol{v}_{b/D}$:[1]

$$\boldsymbol{j}_b = n_b\hbar\nabla\phi_b - \rho_{\mathrm{dr}}\left(\overbrace{\frac{\hbar\nabla\phi_b}{m_b}}^{\boldsymbol{v}_b} - \overbrace{\frac{\hbar\nabla\phi_D}{m_D}}^{\boldsymbol{v}_D} \right), \qquad (11a)$$

$$\boldsymbol{j}_D = n_D\hbar\nabla\phi_D - \rho_{\mathrm{dr}}\left(\frac{\hbar\nabla\phi_D}{m_D} - \frac{\hbar\nabla\phi_b}{m_b} \right). \qquad (11b)$$

Here we consider the Yb wave function (Li dimer wave function), $\psi_b = \sqrt{n_b}e^{i\phi_b}$ ($\psi_D = \sqrt{n_D}e^{i\phi_D}$), and n_b (n_D) is the density of the bosonic (dimer) homogeneous state.

The barrier prevents any flow of the bosons, $\boldsymbol{j}_b = 0$, but the entrainment still allows the accumulation of a phase shift in the presence of fermionic flow $\boldsymbol{j}_D \neq 0$:

$$\frac{\hbar\nabla\phi_b}{m_b} = -\frac{\hbar\nabla\phi_D}{m_D}\frac{\rho_{\mathrm{dr}}}{m_b n_b}\left(1 - \frac{\rho_{\mathrm{dr}}}{m_b n_b}\right)^{-1}, \qquad (12a)$$

$$\boldsymbol{j}_D = n_D\hbar\nabla\phi_D\underbrace{\left[1 - \frac{\rho_{\mathrm{dr}}}{m_D n_D}\left(1 - \frac{\rho_{\mathrm{dr}}}{m_b n_b}\right)^{-1}\right]}_{m_D/m_D^*}. \qquad (12b)$$

Thus, a circulating fermionic superfluid with $\boldsymbol{j}_D \neq 0$ will induce a phase gradient $\nabla\phi_b \approx -\rho_{\mathrm{dr}}\boldsymbol{j}_D/\hbar n_b n_D m_D$ in the

---

[1] In this case, where the momentum operators appear in the functional (7) at only quadratic order, these group velocities can be obtained simply as the derivative of the appropriately defined dispersion: $v_{b,D} = \partial E(\hbar k_b, \hbar k_D)/\partial(\hbar k_{b,D})$. The presence of higher derivatives complicates this, and one must compute the proper momentum currents in terms of the symmetrically ordered expansion of these derivatives.
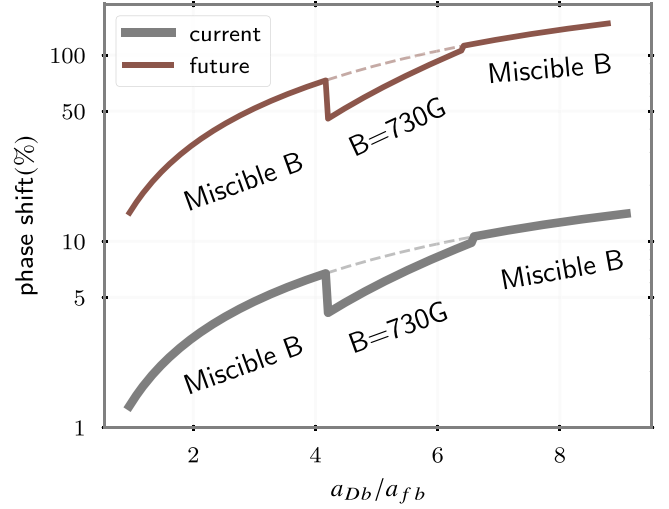

FIG. 3. Entrainment phase shift $\Delta\theta/2\pi$ calculated with magnetic-field B values from the miscibility criterion (8) for a range of values for a_{Db}/a_{fb}. The top (bottom) set of curves is for the future (current) values of parameters in Table I. The dashed region is the high-loss region. For those a_{Db} values, we recommend $B = 730$ G, for which the mixture remains miscible. The phase-shift data are plotted on a logarithmic scale. The points represent the phase-shift values calculated using Eq. (17) at the fiducial points in Table I.

bosons, despite the fact that the barrier keeps the bosonic cloud stationary, $\boldsymbol{j}_b = 0$:

$$\hbar n_b\nabla\phi_b = -\boldsymbol{j}_D\frac{\rho_{\mathrm{dr}}}{m_D n_D}\left[1 - \frac{\rho_{\mathrm{dr}}}{m_D n_D}\left(1 + \frac{m_D n_D}{m_b n_b}\right)\right]^{-1}. \qquad (13)$$

Once the phase shift has been imprinted on the bosons and the fermions have been removed, the bosonic cloud can be released, allowing the opposite sides of the barrier to expand into each other, forming an interference pattern shifted by the relative phase imprint from entrainment. Crucial to the success of this protocol is minimization of contamination from mean-field effects, which, as we mentioned in the Introduction, can be several orders of magnitude larger than the corresponding entrainment effects, precluding observation through other methods such as the dipole frequency shift in a harmonic trap. To mitigate this, our setup develops the phase shift in a homogeneous background around the ring geometry. We have verified through our simulations that the backreaction from the barrier in the bosonic cloud does not induce any mean-field effects, despite the fermionic flow. It will also be crucial to remove the fermionic cloud with a sudden vertical laser pulse before performing the interferometry. Repeating the experiment with circulation in the opposite direction can be used to test for and mitigate any asymmetry in the underlying trap geometry. Numerical values for the proposed experiment are provided in Sec. V (see also Fig. 3).

IV. ESTIMATED PHASE SHIFT

To estimate the phase shift, we consider a homogeneous gas with wave functions

$$\psi_D(\boldsymbol{x}) = \sqrt{n_D}e^{i\boldsymbol{k}_D \cdot \boldsymbol{x}}, \qquad \psi_b(\boldsymbol{x}) = \sqrt{n_b}e^{i\boldsymbol{k}_b \cdot \boldsymbol{x}}, \qquad (14)$$

with $k_{D,b} = \nabla\phi_{D,b}$. In our ring geometry, $k_D = N_w/R$, where N_w is the number of phase windings and R is the radius of the ring. Physically, the magnitude of the winding will be limited by the speed of sound in the superfluid, which defines the local Landau critical velocity v_c which follows from the linearized form of (4), $v_c \approx E_{\mathrm{ph}}(\hbar k)/\hbar k \approx E'_{\mathrm{ph}}(\hbar k)$:

$$v_D = \frac{\hbar k_D}{m_f} < v_c \approx \sqrt{\frac{n_D}{m_D} 4\mathcal{E}''_f(n_f)}. \tag{15}$$

Minimizing (9b), we obtain the induced phase gradient in the bosonic component and the corresponding fractional phase shift

$$\left|\frac{\Delta\theta}{2\pi}\right| = \frac{2\pi R \nabla\phi_b}{2\pi} = \nabla\phi_D \frac{R\rho_{\mathrm{dr}}}{m_D n_b}\left(1 - \frac{\rho_{\mathrm{dr}}}{m_b n_b}\right)^{-1} \tag{16}$$

can be as large as 67%, as we show in the next section.

V. SIMULATIONS

We first verify our model by calculating the dipole oscillation frequency of the bosonic cloud in a Yb-Li superfluid mixture using the experimental parameters of [42]. In this experiment, a small Yb BEC oscillates in a large ^{6}Li cloud at $B = 780$ G in a stable mixture of two superfluids featuring large mass mismatch and distinct electronic properties. In principle, the entrainment terms should modify the oscillation frequency from that of the background harmonic trap, but as discussed in the Introduction, this shift is two orders of magnitude smaller than the shift due to the mean-field interaction.

As validation of our mean-field implementation, we reproduce the observations in [42], obtaining a frequency shift of dipole oscillation consistent with the measured values. We include the trap offset in the direction of the gravity and use $a_{Db} = 2a_{fb}$.

In the presence of the Li cloud, the dipole oscillation frequency ω_d of the Yb BEC is extracted to be $2\pi \times 381.3(4)$ Hz. From our calculation, the frequency is $2\pi \times 381.4(9)$ Hz, well within the experimental errors. In the experiment, along with the center-of-mass (c.m.) mode, scissor modes get excited. The absence of the growth of the scissor mode shows very small energy transfer from the c.m. mode. Our simulations capture the same qualitative effect.

A subtle point in the experiment was the observation of a decay in the amplitude of the dipole mode. In Ref. [42] it was conjectured that this may be due to the excitation of quadrupole modes to which the dipole mode is coupled by anharmonicity in the trapping potential. Within our model, we find that the frequencies of the two modes are sufficiently distinct that energy cannot be efficiently transferred and suggest instead that this dissipation is due to thermal effects. We can reproduce the measured decay constants $\omega_d\tau$ within our DGPE model (10) with a phase of $\eta \approx 0.0015$. The measured and calculated values are 250 and 210, respectively, which are in reasonable agreement.

Aside from this effect, we reproduce the results with our self-consistent model, verifying the excitation and behavior of scissor modes from misalignment in the trap, and the mean-field frequency shifts. This validates that our model properly captures the mean-field effects which can potentially obscure entrainment signals. We use this model to simulate the proposed experimental procedure to detect entrainment as described in Sec. III, including all mean-field effects and density inhomogeneities due to the trapping potentials. An important part of this validation is that the induced flow in the fermionic superfluid coupled with the bosonic density perturbation from the barrier *does not* produce an asymmetry in density across the barrier. This lack of density asymmetry differentiates, for example, superfluid entrainment from mutual friction [100]: The latter would drag and change the mean-field densities. The main difference is that entrainment interaction couples the gradients of the phases of the two wave functions. Therefore, once the transient fluctuations die off, we will have a persistent flow in the fermionic component, which will induce a phase gradient on the bosons, leading to a velocity difference across the barrier. Once we remove the barrier in the bosonic component and let the two parts of the cloud expand into each other, the velocity difference will result in a shift in the interference pattern. We may detect this shift by comparing against the interference fringes produced in a system without the induced phase gradient.

A. Experimental parameters

We present our results in terms of two sets of parameters: a current set of parameter values that have been demonstrated through various existing experiments and a future set of realistic parameter values optimized to detect the entrainment effect. We find that with current parameters, a modest phase shift occurs which lies at the bounds of current detectability; however, with future improvements, a significant phase shift will be induced that should enable the first direct detection of superfluid entrainment.

1. Current parameters

Current experiments in ring traps have demonstrated the ability to trap $N_b \approx 10^5$ bosonic atoms [96] and recently approximately 10^4 fermionic atoms [101]. In harmonic traps $N_b = N_f \approx 10^5$ has been achieved in a Fermi-Bose mixture [41,42] and $N_f \approx 10^6$–10^7 has been reported for single species [102]. With current technology, we expect experimental improvements to trap higher numbers of fermions in the near future.

The main limit on the maximum density is particle loss due to three-body processes which scale as n^3. We can mitigate this to some extent by adjusting the fermion density with the magnetic field and the boson density with the trap frequencies. For our analysis, we fix the trap frequency for the bosons at $2\pi \times 400$ Hz. This gives a lifetime for the Yb BEC of approximately 2 s [103] with a central density approximately equal to 340 μm^{-3} $\approx 3.4 \times 10^{14}$ cm^{-3} and chemical potential $\mu_b \approx 65$ nK ($\mu_b/\hbar\omega_{Yb} \approx 3$) in a 30-$\mu$m trap. Excessively tight traps can heat the system, reducing the expected lifetime. We propose using the same laser to trap both chemical species, which limits the relative polarizability α between the two species. With $\alpha = 6.2$, at 638 G, the trap frequency for fermions becomes approximately equal to $2\pi \times 5$ kHz, setting the lifetime of Li dimers at approximately 107 ms with chemical potential $\mu_D \approx 1.43$ μK ($\mu_D/\hbar\omega_{Li} \approx 5$) and central density approximately equal to 100 μm^{-3} $\approx 1 \times 10^{14}$ cm^{-3}.

TABLE II. Extracted parameter dependence for current and future parameter values. These are the powers p appearing in corresponding terms of Eq. (17). The errors express the typical range over which the exponents vary when the parameters are changed by $\pm 10\%$ about the current or future values listed in Table I.

Parameter	Current exponent	Future exponent
$\alpha/6.2$	0.592 03(2)	0.564 86(3)
$N_b/10^5$	$-0.031(3)$	$-0.034(3)$
$N_f/10^5$	0.592 02(2)	0.564 86(3)
$m_b m_f/m_{Yb} m_{Li}$	0.5609(1)	0.5308(1)
$R/30\ \mu m$	0.4391(1)	0.4691(1)
$B/638$ G	$-3.18(5)$	$-3.67(2)$
$a_{Db}/3.87 a_{fb}$	2.0152(2)	2.0279(3)
$(m_b/m_f)/(m_{Yb}/m_{Li})$	0.02(1)	0.03(1)

Here the Yb-Li scattering length remains roughly constant.[2] These densities are dilute in the sense that mean-field analyses are valid. Standard values for relevant scattering lengths in the system are $a_{bb} = 5.5$ nm, the boson-boson scattering length [105], and $a_{fb} = 1.59$ nm, the fermion-boson scattering length [87].

In Table I we compare two sets of adjustable parameters. In the table, v/v_c corresponds to the flow velocity as a fraction of Landau critical velocity in Li, ξ is the Bertsch parameter, and the rest of the parameters have their usual meanings. The left-hand side of the first column shows typical values realized in current experiments. The right-hand side shows how these could be adjusted to maximize the entrainment signal with values that should be attainable with reasonable experimental advances.

We have calculated the percentage phase shift from unitarity up to the BEC side of the phase diagram for the Fermi-Bose mixture by numerically integrating Eq. (28) of [14] at $T = 0$ with a modified equation of state and phonon dispersion relationship for the fermionic dimers. We have also determined the parameter dependences of the percentage phase shift from scaling analysis and it has the following form:

$$\frac{\Delta\theta}{2\pi} \approx (6.2\%)\left(\frac{v}{0.15 v_c}\right)\left(\frac{a_{Db}}{3.87 a_{fb}}\right)^{2.02(1)}\left(\frac{B}{638\text{ G}}\right)^{-3.4(3)}$$

$$\times \left(\frac{\alpha}{6.2}\right)^{0.58(1)}\left(\frac{R}{30\ \mu m}\right)^{0.46(1)}\left(\frac{N_f}{10^5}\right)^{0.58(1)}$$

$$\times \left(\frac{N_b}{10^5}\right)^{-0.033(1)}\left(\frac{m_b m_f}{m_{Yb} m_{Li}}\right)^{0.54(1)}\left(\frac{m_b/m_f}{m_{Yb}/m_{Li}}\right)^{0.02(1)}.$$

$$(17)$$

The exponents in Eq. (17) demonstrate the approximate dependence of the phase shift on various parameters. The errors in the exponents demonstrate how the exponents vary due to the full functional dependence provided in the accompanying code [89,90], accounting for the changes in values for the currently achievable parameters (left column in Table I) from the possible experimental parameters implementable in the

future (right column in Table I). See Table II for a complete tabulation of these exponents and their errors.

2. Future parameters

From Eq. (17) we see that the most significant signal enhancements come from increasing the dimer-boson scattering length a_{Db} and decreasing the magnetic field B towards the BEC limit. Miscibility limits the enhancement of these two effects, requiring one to adjust the magnetic field B according to Eq. (8). To maximize the entrainment signal, one should use the lowest magnetic field allowed by miscibility (see Fig. 1), but particle loss rates are particularly high in the range 650–720 G [88]. At each magnetic field, the miscibility condition gives us values of a_{Db} for which the mixture remains miscible. If the unknown a_{Db} value lies within the miscible a_{Db} range of 650–720 G, then one should keep $B \approx 730$ G to minimize particle loss.

Other parameters that have a positive effect on the enhancement are the radius of the ring R and the induced flow velocity v/v_c. In general, by increasing each of them we can increase the signal strength, but each of them is limited by potential experimental challenges. Perfect larger ring traps are harder to obtain as they may not remain flat at the center along the azimuthal axis. This will lead to production of a higher amount of mean-field density fluctuation which may not completely die out within the lifetime of the metastable superfluid state. For a single bosonic species $R \approx 250\ \mu m$ [106] has been achieved. This order of magnitude may be achievable for a superfluid mixture. In our experimental protocol, creating a substantial flow in the fermionic component increases the signal strength by a considerable amount, but is strictly limited by the number of windings we can induce set by Landau criterion. There is also the possibility to make an improvement by increasing the induced velocity to as close as possible to the critical velocity. Typically, only approximately 10% of the critical velocity is accessed [107], but recent experiments have achieved much higher induced flow velocities, which could potentially increase the detectable entrainment signal [108]. A key part of our protocol is to used the same ring trap for both species, which will ensure they are trapped in the same physical space. The centrifugal force of the rotating fluid displaces the fermionic cloud slightly, but with these parameters the displacement is insignificant, less than approximately $0.014\ \mu m$.

With the current parameter set, we may produce a phase shift up to approximately 6% (considering the mean-field enhancement of a_{Db}) of observable phase shift. The suggested improvements (future parameters) may increase the signal to as high as approximately 67%.

B. Entrainment signal

We present snapshots from the one-dimensional time evolution of the bosonic component in a tube with the current and future parameters in Fig. 4. These are time evolution images, which demonstrate the asymmetry in the interference fringes generated from the entrainment interaction. In an actual experimental procedure, the interfering clouds will be imaged after a time-of-flight expansion after turning off the confining potential, where the density will drop and the mean-field

---

[2]Narrow Feshbach resonances (less than 1 mG) have recently been observed in Yb-Li mixtures [104]. These do not affect our discussion.
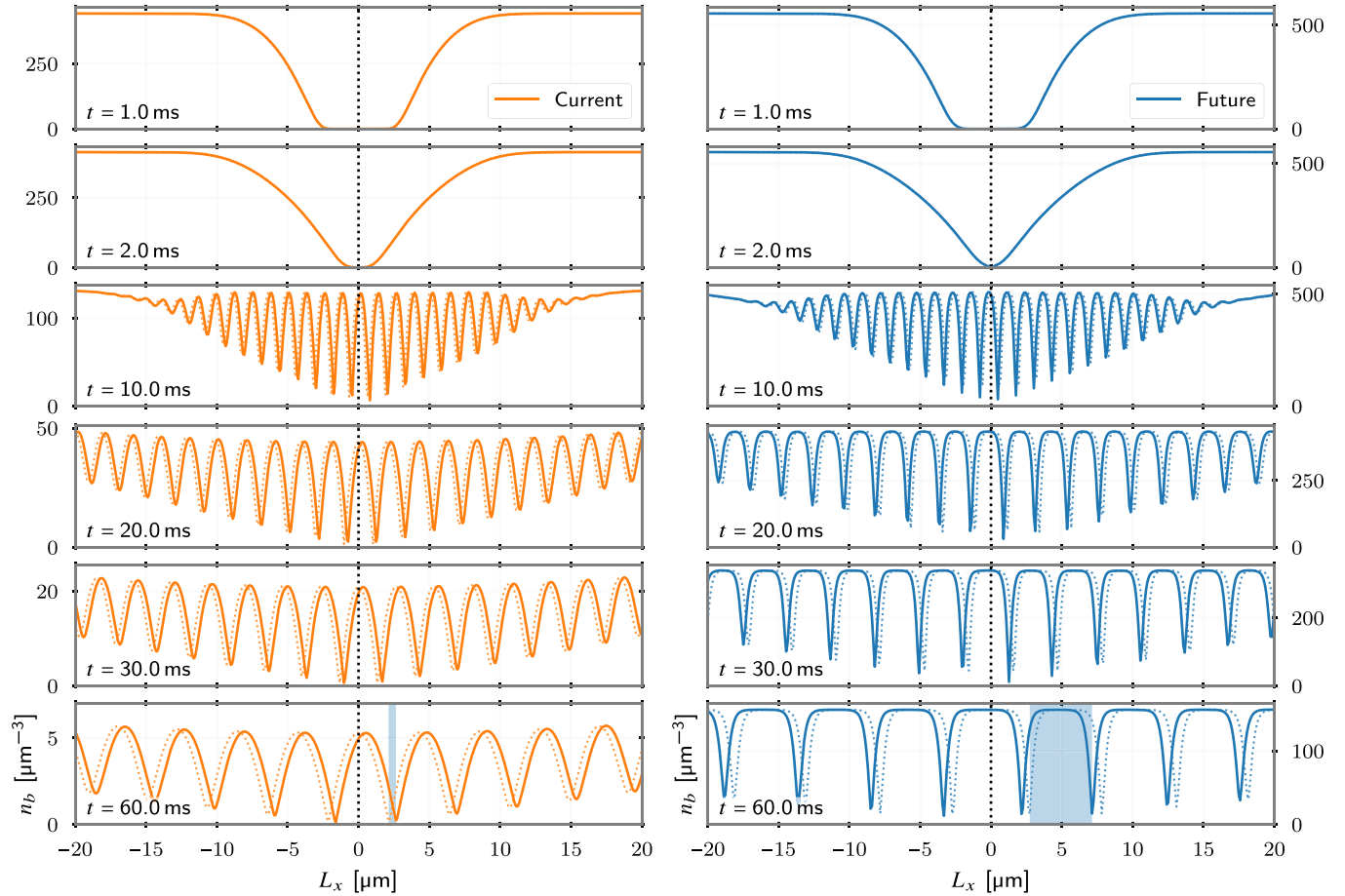
FIG. 4. Free expansion of the central density of the bosonic component of the mixture in a periodic box, using the current parameter set (left) and future parameters (right) (see Table I). Notice the asymmetry around the vertical line at $L_x = 0$: a signature of the measurable entrainment shift. These expansion simulations are done with full three-dimensional parameters in a tube geometry, which reduces the complexity of the numerical calculations significantly while having the essential aspects of the full three-dimensional calculation. Consequently, they do not capture the full radial expansion of the ring, but mimic the density drop. Back to back measurements will also make the signal more comparable to the expansion of a state without asymmetry. In the calculations here, we have used $a_{Db} = 3.87a_{fb}$ and chose the two parts of the cloud to be separated approximately 6 μm. The dotted lines represent the expansion without any entrainment effect, to distinguish the amount of the shift. The lightly shaded region in the bottom right panel shows the amount of shift approximately equal to 5 μm.

interaction between the bosons will be reduced. In that scenario, the fringe spacing after a long expansion time t is

$$\lambda_s \approx \frac{2\pi\hbar t}{md} \qquad (18)$$

for initial separation d, as seen in the earlier experiments [99]. Essentially, with long time-of-flight expansion, the fringe spacing increases linearly with time and 30 ms is typical for earth-bound laboratory experiments. This can be increased by a factor of 3–10 in a microgravity setting [109] as the reduced gravity will substantially increase the time of flight. By employing a linear optical potential (with a laser far detuned from the Yb resonances), one may also reduce the effect of gravity and increase the time of flight [110]. Competing factors here are the initial separation and the mean-field interaction. The clouds have to be initially separated enough that they can grow large in size before the interference. Therefore, a point of suitable compromise has to be reached to maximize the signal in a typical laboratory experiment. The reduction in density during the time of flight has another positive effect

on the experimental outcome. This widens the fringes, which will make them easier to resolve. To demonstrate this effect we perform simulations in a tube geometry, which mimics the density reduction in a radially expanding cloud. A similar effect is also visibly present in the two-dimensional expansion of the ring in Fig. 5.

Finite-temperature effects could impact our estimates in two ways. The presence of a thermal component will reduce the contrast, filling in the interference fringes. As demonstrated in Ref. [99], however, with achievable temperatures, the reduction in contrast is not significant. Furthermore, the thermal cloud will disperse more quickly during the time-of-flight expansion time from 30 to 50 ms, enhancing the signal.

The thermal cloud will also reduce the fraction of condensate, impacting the entrainment signal. From the scaling relationship (17), we see that $T/T_c \approx 0.55$ [42] would result in an approximately 11% reduction in the percentage phase shift. Thus, as long as the imprinting procedure does not overly heat the system, there should be plenty of contrast.
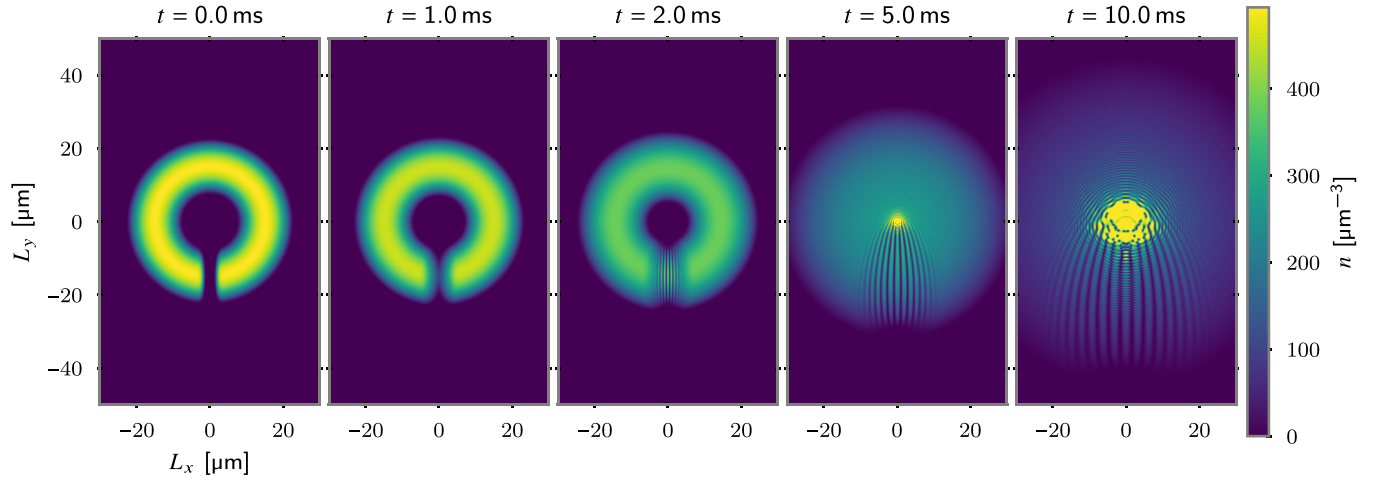
FIG. 5. Schematic radial expansion of a ring with an induced phase gradient in the bosonic component. As time progresses (left to right), the density decreases because of the outward radial expansion and the fringes become wider. (This is schematic in the sense that it is in an effective two-dimensional geometry with translation invariance out of the page and the visual effect is enhanced by increasing the density.)

VI. CONCLUSION

We proposed an experimental protocol to directly measure for the bulk three-dimensional entrainment, the Andreev-Bashkin effect, in a fermionic and bosonic superfluid mixture. By using a ring geometry with a common trap for both species, we demonstrated that atom interferometry techniques can produce measurable phase shifts with reasonable experimental parameters and we characterized their dependence. An important feature of our protocol is the elimination of mean-field effects, which have thwarted previous attempts to measure entrainment based on shifts in the dipole oscillation frequency in a harmonic trap. The broad Feshbach resonance allows us to adjust the interaction strength of the ^{6}Li superfluid to ensure miscibility and the large mass of the bosonic ^{174}Yb superfluid enhances the entrainment effect. One uncertainty is the dimer-boson scattering length a_{Db}, which may have significant corrections from three-body physics [84]. The value of this parameter still needs careful measurement, but a significant enhancement to the entrainment signal is possible if this is large, introducing an intriguing potential for developing a significant entrainment effect by tuning three-body interactions. With current technologies and assuming mean-field values for a_{Db}, a 6% phase shift should be reliable. With reasonable improvements in experimental techniques, this may be as large as 67%.

ACKNOWLEDGMENTS

APPENDIX

1. Radial expansion

Here we demonstrate snapshots from a schematic radial expansion of a ring in two dimensions in Fig. 5. This simu-

lation is done with the current parameters in Table I, except we modified the density and the width of the ring to enhance the interference effect, allowing more visibility for the demonstration purpose. This demonstration reiterates the importance of time-of-flight expansion in the detection procedure. Longer time-of-flight expansion make the fringes easier to resolve by increasing the fringe width.

2. Deviations in the exponents

Table II shows the deviation in the exponents that appear in Eq. (17).

3. Equation of state: ^{6}Li

To perform our calculations, we parametrize the equation of state of ^{6}Li Fermi gas. Once we fix the scattering length a_{Li}, in terms of the external magnetic field B, we use the model

$$\mathcal{E}(n, x) = f(x)\mathcal{E}_{FG}(n), \tag{A1a}$$

$$f(x) = \frac{bx + \xi}{\frac{x}{\xi}(b + \zeta) + 1 + \frac{18\pi bx^2}{5a_{DD}/a_{\mathrm{Li}}}}, \tag{A1b}$$

with $x = 1/k_F a$ and $\mathcal{E}_{FG}(n) = \frac{3}{5}n\hbar^2 k_F^2/2m_F$. This Padé expansion has two limits:

$$\frac{\mathcal{E}(n)}{\mathcal{E}_{FG}(n)} = \begin{cases} \xi - \zeta x + O(x^2), & x \approx 0 \text{ (unitarity)} \\ -\frac{5}{3}x^2 + \frac{a_{DD}}{a_{\mathrm{Li}}}\frac{5}{18\pi x} + O(\frac{1}{x^2}), & x \to \infty \text{ (BEC)}. \end{cases}$$

Here a_{DD} is the dimer-dimer scattering length ($a_{DD} = 0.6a_{\mathrm{Li}}$), ζ is the contact ($\zeta \approx 0.901$), and ξ is the Bertsch parameter [$\xi = 0.3742(5)$]. The more relevant parameter in this case, the dimer-dimer scattering length, is calculated using $a_{DD} = 0.6a_{\mathrm{Li}}$ [71].

In the BEC limit, this reproduces the expected equation of state for a BEC of dimers with density $n_D = n/2$, mass $m_D = 2m_F$, and scattering length a_{DD}. The value of $b = 0.25$ is chosen to match the QMC data on the BEC side of the phase

diagram:

$$\mathcal{E}_{\text{BEC}}(n) = -\frac{\hbar^2}{2m_F a_{\text{Li}}^2}n + \frac{g_{DD}n_D^2}{2} + \cdots , \quad g_{DD} = \frac{4\pi\hbar^2 a_{DD}}{m_D}.$$

To relate the magnetic-field strength B with the scattering length, we fit the data from [77], using the model from [111]:

$$a_{\text{Li}}^{-1} = a_{bg}^{-1}\frac{B - B_0}{(B - B_0 + \Delta)[1 + \alpha(B - B_0)]},$$

$$B_0 = 832.178\,498\,\text{G}, \quad \Delta = 293.396\,620\,\text{G},$$

$$a_{bg} = -1415.051\,08 a_B, \quad \alpha = 0.000\,406\,405\,370,$$

$$a_B = 0.052\,917\,7\,\text{nm}. \tag{A2}$$

4. Entrainment coefficient

We have used Eq. (28) of [14] at $T = 0$ as ρ_{dr} in our calculation. The analytic form is

$$\rho_{\text{dr}} = \int \frac{dk}{2\pi^2}k^2\gamma_{Db}^2\sqrt{m_D m_b}\frac{n_D n_b(\epsilon_D\epsilon_b)^{3/2}}{\Omega_D\Omega_b(\Omega_D + \Omega_b)^3}, \tag{A3}$$

with

$$\epsilon_i = \frac{\hbar^2 k^2}{2m_i}, \quad E_i = \epsilon_i(\epsilon_i + 2g_i n_i),$$

$$\gamma_{Db} = \frac{2\pi\hbar^2 a_{Db}(m_D + m_b)}{m_D m_b},$$

$$g_{bb} = \frac{4\pi\hbar^2 a_{bb}}{m_b}, \quad g_{DD} = \frac{\partial^2\mathcal{E}_f(2n_D)}{\partial n_D^2},$$

and

$$\Omega_i = \left(\frac{E_b^2 + E_D^2}{2} \pm \sqrt{\frac{(E_b^2 - E_D^2)^2}{4} + 4\gamma_{Db}^2 n_D n_b\epsilon_D\epsilon_b}\right)^{1/2}.$$

We have numerically verified that, in the regions of experimental interest,

$$\rho_{\text{dr}} \approx \int \frac{dk}{2\pi^2}k^2\gamma_{Db}^2\sqrt{m_D m_b}\frac{n_D n_b}{\Omega_D\Omega_b} \tag{A4}$$

follows similar scaling relationships as ρ_{dr} and can be used to intuitively understand the scaling relationship shown in Eq. (17). The essence is that, in the integral, the complicated cubic dependences essentially drop out and we can use the simplified relationship for qualitative discussions and rough estimates of the scaling exponents. For quantitative results, we numerically integrate ρ_{dr} in the thermodynamic limit for homogeneous matter with all dependences. To estimate the finite-size effects from the confinement of the ring, we compute the integrals as momentum sums in a finite periodic box and find only a small correction of 1.86%–2.5% for future and current parameters, respectively. For completeness, we write the explicit parameter dependences $\gamma_{Db}(a_{Db}, m_D, m_b)$, $n_D(N_f, m_f, R, \omega_f, \xi, B)$, $n_b(N_b, m_b, \omega_b, a_{bb}, R)$, and $\omega_f(\alpha, \omega_b)$.

[1] A. F. Andreev and E. P. Bashkin, Three-velocity hydrodynamics of superfluid solutions, Zh. Eksp. Teor. Fiz. **69**, 319 (1975) [Sov. Phys. JETP **42**, 164 (1975)].

[2] G. E. Volovik, V. P. Mineev, and I. M. Khalatnikov, Theory of solutions of a superfluid Fermi liquid in a superfluid Bose liquid, Zh. Eksp. Teor. Fiz. **69**, 675 (1975) [Sov. Phys. JETP **42**, 342 (1975)].

[3] N. Chamel, Superfluidity and superconductivity in neutron stars, J. Astrophys. Astron. **38**, 43 (2017).

[4] B. Haskell and A. Sedrakian, in *The Physics and Astrophysics of Neutron Stars*, edited by L. Rezzolla, P. Pizzochero, D. I. Jones, N. Rea, and I. Vidaña (Springer, Cham, 2018), pp. 401–454.

[5] M. Antonelli and P. M. Pizzochero, Pulsar rotation with superfluid entrainment, J. Phys.: Conf. Ser. **861**, 012024 (2017).

[6] L. B. Leinson, Non-linear approach to the entrainment matrix of superfluid nucleon mixture at zero temperature, Mon. Not. R. Astron. Soc. **470**, 3374 (2017).

[7] A. Bulgac, M. M. Forbes, S. Jin, R. N. Perez, and N. Schunck, Minimal nuclear energy density functional, Phys. Rev. C **97**, 044313 (2018).

[8] J. Nespolo, G. E. Astrakharchik, and A. Recati, Andreev-Bashkin effect in superfluid cold gases mixtures, New J. Phys. **19**, 125005 (2017).

[9] L. Parisi, G. E. Astrakharchik, and S. Giorgini, Spin Dynamics and Andreev-Bashkin Effect in Mixtures of One-Dimensional Bose Gases, Phys. Rev. Lett. **121**, 025302 (2018).

[10] F. Chevy, Counterflow in a doubly superfluid mixture of bosons and fermions, Phys. Rev. A **91**, 063606 (2015).

[11] L. Y. Kravchenko and D. V. Fil, Critical currents and giant nondissipative drag for superfluid electron hole pairs in quantum Hall multilayers, J. Phys.: Condens. Matter **20**, 325235 (2008).

[12] D. V. Fil and S. I. Shevchenko, Drag of superfluid current in bilayer Bose systems, Low Temp. Phys. **30**, 770 (2004).

[13] D. V. Fil and S. I. Shevchenko, Berry phase caused by nondissipative drag of superflow in a Bose qubit, arXiv:cond-mat/0404567.

[14] D. V. Fil and S. I. Shevchenko, Nondissipative drag of superflow in a two-component Bose gas, Phys. Rev. A **72**, 013616 (2005).

[15] M. V. Demin, Y. E. Lozovik, and V. A. Sharapov, Bose condensate drag in a system of two coupled traps, JETP Lett. **76**, 135 (2002).

[16] A. Syrwid, E. Blomquist, and E. Babaev, Drag-induced dynamical formation of dark solitons in Bose mixture on a ring, arXiv:2203.06756.

[17] C. Chin, R. Grimm, P. Julienne, and E. Tiesinga, Feshbach resonances in ultracold gases, Rev. Mod. Phys. **82**, 1225 (2010).

[18] N. Chamel, Viewpoint: A stellar superfluid, Physics **4**, 14 (2011).

[19] P. W. Anderson and N. Itoh, Pulsar glitches and restlessness as a hard superfluidity phenomenon, Nature (London) **256**, 25 (1975).

[20] M. A. Alpar, Pinning and threading of quantized vortices in the pulsar crust superfluid, Astrophys. J. **213**, 527 (1977).

[21] P. B. Jones, Rotation of the neutron-drip superfluid in pulsars: The interaction and pinning of vortices, Astrophys. J. **373**, 208 (1991).

[22] B. K. Link and R. I. Epstein, Mechanics and energetics of vortex unpinning in neutron stars, Astrophys. J. **373**, 592 (1991).

[23] B. Link, R. I. Epstein, and J. M. Lattimer, Pulsar Constraints on Neutron Star Structure and Equation of State, Phys. Rev. Lett. **83**, 3362 (1999).

[24] M. Mannarelli, K. Rajagopal, and R. Sharma, The Rigidity of crystalline color superconducting quark matter, Phys. Rev. D **76**, 074026 (2007).

[25] P. M. Pizzochero, Angular momentum transfer in Vela-like pulsar glitches, Astrophys. J. Lett. **743**, L20 (2011).

[26] N. Andersson, B. Haskell, and L. Samuelsson, Lagrangian perturbation theory for a superfluid immersed in an elastic neutron star crust, Mon. Not. R. Astron. Soc. **416**, 118 (2011).

[27] N. Andersson, K. Glampedakis, W. C. G. Ho, and C. M. Espinoza, Pulsar Glitches: The Crust is not Enough, Phys. Rev. Lett. **109**, 241103 (2012).

[28] L. Warszawski and A. Melatos, Gross-Pitaevskii model of pulsar glitches, Mon. Not. R. Astron. Soc. **415**, 1611 (2011).

[29] F. Grill and P. Pizzochero, Vortex-lattice interaction in Pulsar Glitches, J. Phys.: Conf. Ser. **342**, 012004 (2012).

[30] L. Warszawski and A. Melatos, Knock-on processes in superfluid vortex avalanches and pulsar glitch statistics, Mon. Not. R. Astron. Soc. **428**, 1911 (2013).

[31] A. Melatos and B. Link, Pulsar timing noise from superfluid turbulence, Mon. Not. R. Astron. Soc. **437**, 21 (2014).

[32] C. A. van Eysden, and A. Melatos, Spin-up of a two-component superfluid: Analytic theory in arbitrary geometry, J. Fluid Mech. **729**, 180 (2013).

[33] P. D. Lasky, M. F. Bennett, and A. Melatos, Stochastic gravitational wave background from hydrodynamic turbulence in differentially rotating neutron stars, Phys. Rev. D **87**, 063004 (2013).

[34] N. Chamel, Crustal Entrainment and Pulsar Glitches, Phys. Rev. Lett. **110**, 011101 (2013).

[35] S. Seveso, P. M. Pizzochero, F. Grill, and B. Haskell, Mesoscopic pinning forces in neutron star crusts, Mon. Not. R. Astron. Soc. **455**, 3952 (2016).

[36] R. F. Archibald, V. M. Kaspi, C. Y. Ng, K. N. Gourgouliatos, D. Tsang, P. Scholz, A. P. Beardmore, N. Gehrels, and J. A. Kennea, An anti-glitch in a magnetar, Nature (London) **497**, 591 (2013).

[37] A. Lyne, C. Jordan, F. Graham-Smith, C. Espinoza, B. Stappers, and P. Weltrvrede, 45 years of rotation of the Crab pulsar, Mon. Not. R. Astron. Soc. **446**, 857 (2015).

[38] B. Haskell and A. Melatos, Models of pulsar glitches, Int. J. Mod. Phys. D **24**, 1530008 (2015).

[39] E. Babaev, Andreev-Bashkin effect and knot solitons in an interacting mixture of a charged and a neutral superfluid with possible relevance for neutron stars, Phys. Rev. D **70**, 043001 (2004).

[40] G. Modugno, M. Modugno, F. Riboli, G. Roati, and M. Inguscio, Two Atomic Species Superfluid, Phys. Rev. Lett. **89**, 190404 (2002).

[41] I. Ferrier-Barbut, M. Delehaye, S. Laurent, A. T. Grier, M. Pierce, B. S. Rem, F. Chevy, and C. Salomon, A mixture of Bose and Fermi superfluids, Science **345**, 1035 (2014).

[42] R. Roy, A. Green, R. Bowler, and S. Gupta, Two-Element Mixture of Bose and Fermi Superfluids, Phys. Rev. Lett. **118**, 055301 (2017).

[43] A. G. Truscott, K. E. Strecker, W. I. McAlexander, G. B. Partridge, and R. G. Hulet, Observation of Fermi pressure in a gas of trapped atoms, Science **291**, 2570 (2001).

[44] V. Graber, N. Andersson, and M. Hogg, Neutron stars in the laboratory, Int. J. Mod. Phys. D **26**, 1730015 (2017).

[45] J. Tuoriniemi, J. Martikainen, E. Pentti, A. Sebedash, S. Boldarev, and G. Pickett, Towards superfluidity of ^{3}He diluted by ^{4}He, J. Low Temp. Phys. **129**, 531 (2002).

[46] J. Rysti, J. Tuoriniemi, and A. Salmela, Effective ^{3}He interactions in dilute ^{3}He-^{4}He mixtures, Phys. Rev. B **85**, 134529 (2012).

[47] T. S. Riekki, A. P. Sebedash, and J. T. Tuoriniemi, Thermodynamics of adiabatic melting of solid ^{4}He in liquid ^{3}He, Phys. Rev. B **99**, 054502 (2019).

[48] S. I. Shevchenko and D. V. Fil, The Andreev-Bashkin effect in a two-component Bose gas, J. Exp. Theor. Phys. **105**, 135 (2007).

[49] M. Abad, A. Recati, S. Stringari, and F. Chevy, Counter-flow instability of a quantum mixture of two superfluids, Eur. Phys. J. D **69**, 126 (2015).

[50] T. Ozawa, A. Recati, M. Delehaye, F. Chevy, and S. Stringari, Chandrasekhar-Clogston limit and critical polarization in a Fermi-Bose superfluid mixture, Phys. Rev. A **90**, 043608 (2014).

[51] Y. Liao, A. S. C. Rittner, T. Paprotta, W. Li, G. B. Partridge, R. G. Hulet, S. K. Baur, and E. J. Mueller, Spin-imbalance in a one-dimensional Fermi gas, Nature (London) **467**, 567 (2010).

[52] G. B. Partridge, W. Li, R. I. Kamar, Y. Liao, and R. G. Hulet, Pairing and phase separation in a polarized Fermi gas, Science **311**, 503 (2006).

[53] J. M. Midtgaard, Z. Wu, and G. M. Bruun, Time-reversal-invariant topological superfluids in Bose-Fermi mixtures, Phys. Rev. A **96**, 033605 (2017).

[54] M. Ögren and G. M. Kavoulakis, Rotational properties of superfluid Fermi-Bose mixtures in a tight toroidal trap, Phys. Rev. A **102**, 013323 (2020).

[55] M. Tylutki, A. Recati, F. Dalfovo, and S. Stringari, Dark-bright solitons in a superfluid Bose-Fermi mixture, New J. Phys. **18**, 053014 (2016).

[56] A. Albus, F. Illuminati, and J. Eisert, Mixtures of bosonic and fermionic atoms in optical lattices, Phys. Rev. A **68**, 023606 (2003).

[57] S. Akhanjee, Quasiparticle excitations in Bose-Fermi mixtures, Phys. Rev. B **82**, 075138 (2010).

[58] H. Fehrmann, M. A. Baranov, B. Damski, M. Lewenstein, and L. Santos, Mean-field theory of Bose-Fermi mixtures in optical lattices, Opt. Commun. **243**, 23 (2004).

[59] J. A. Scaramazza, B. Kain, and H. Y. Ling, Competing orders in a dipolar Bose-Fermi mixture on a square optical lattice: mean-field perspective, Eur. Phys. J. D **70**, 147 (2016).

[60] K. Noda, R. Peters, N. Kawakami, and T. Pruschke, Many-body effects in a Bose-Fermi mixture, Phys. Rev. A **85**, 043628 (2012).

[61] K. Sellin and E. Babaev, Superfluid drag in the two-component Bose-Hubbard model, Phys. Rev. B **97**, 094517 (2018).

[62] P. P. Hofer, C. Bruder, and V. M. Stojanović, Superfluid drag of two-species Bose-Einstein condensates in optical lattices, Phys. Rev. A **86**, 033627 (2012).

[63] J. Linder and A. Sudbø, Calculation of drag and superfluid velocity from the microscopic parameters and excitation energies

of a two-component Bose-Einstein condensate in an optical lattice, Phys. Rev. A **79**, 063610 (2009).

[64] D. Contessi, D. Romito, M. Rizzi, and A. Recati, Collisionless drag for a one-dimensional two-component Bose-Hubbard model, Phys. Rev. Research **3**, L022017 (2021).

[65] S. Hartman, E. Erlandsen, and A. Sudbø, Superfluid drag in multicomponent Bose-Einstein condensates on a square optical lattice, Phys. Rev. B **98**, 024512 (2018).

[66] C. H. Schunck, M. W. Zwierlein, C. A. Stan, S. M. F. Raupach, W. Ketterle, A. Simoni, E. Tiesinga, C. J. Williams, and P. S. Julienne, Feshbach resonances in fermionic ^{6}Li, Phys. Rev. A **71**, 045601 (2005).

[67] *The BCS-BEC Crossover and the Unitary Fermi Gas*, edited by W. Zwerger, Lecture Notes in Physics Vol. 836 (Springer, Berlin, 2012).

[68] F. Ancilotto, L. Salasnich, and F. Toigo, Shock waves in strongly interacting Fermi gas from time-dependent density functional calculations, Phys. Rev. A **85**, 063612 (2012).

[69] J. A. Joseph, J. E. Thomas, M. Kulkarni, and A. G. Abanov, Observation of Shock Waves in a Strongly Interacting Fermi Gas, Phys. Rev. Lett. **106**, 150401 (2011).

[70] M. M. Forbes and R. Sharma, Validating simple dynamical simulations of the unitary Fermi gas, Phys. Rev. A **90**, 043638 (2014).

[71] D. S. Petrov, C. Salomon, and G. V. Shlyapnikov, Weakly Bound Dimers of Fermionic Atoms, Phys. Rev. Lett. **93**, 090404 (2004).

[72] M. M. Forbes, S. Gandolfi, and A. Gezerlis, Effective-range dependence of resonantly interacting fermions, Phys. Rev. A **86**, 053603 (2012).

[73] G. F. Bertsch, Many-body X challenge problem (unpublished).

[74] G. A. Baker, Jr., Neutron matter model, Phys. Rev. C **60**, 054311 (1999).

[75] G. A. Baker, Jr., The MBX challenge competition: A neutron matter model, Int. J. Mod. Phys. B **15**, 1314 (2001).

[76] M. J. H. Ku, A. T. Sommer, L. W. Cheuk, and M. W. Zwierlein, Revealing the superfluid lambda transition in the universal thermodynamics of a unitary Fermi gas, Science **335**, 563 (2012).

[77] G. Zürn, T. Lompe, A. N. Wenz, S. Jochim, P. S. Julienne, and J. M. Hutson, Precise Characterization of ^{6}Li Feshbach Resonances Using Trap-Sideband-Resolved RF Spectroscopy of Weakly Bound Molecules, Phys. Rev. Lett. **110**, 135301 (2013).

[78] M. M. Forbes, S. Gandolfi, and A. Gezerlis, Resonantly Interacting Fermions in a Box, Phys. Rev. Lett. **106**, 235303 (2011).

[79] J. Carlson, S. Gandolfi, K. E. Schmidt, and S. Zhang, Auxiliary field quantum Monte Carlo for strongly paired fermions, Phys. Rev. A **84**, 061602(R) (2011).

[80] J. E. Drut, T. A. Lähde, and T. Ten, Momentum Distribution and Contact of the Unitary Fermi Gas, Phys. Rev. Lett. **106**, 205302 (2011).

[81] R. Rossi, T. Ohgoe, E. Kozik, N. Prokof'ev, B. Svistunov, K. Van Houcke, and F. Werner, Contact and Momentum Distribution of the Unitary Fermi Gas, Phys. Rev. Lett. **121**, 130406 (2018).

[82] G. E. Astrakharchik, J. Boronat, J. Casulleras, and S. Giorgini, Equation of State of a Fermi Gas in the BEC-BCS Crossover: A Quantum Monte Carlo Study, Phys. Rev. Lett. **93**, 200404 (2004).

[83] S. K. Adhikari and L. Salasnich, Effective nonlinear Schrödinger equations for cigar-shaped and disc-shaped Fermi superfluids at unitarity, New J. Phys. **11**, 023011 (2009).

[84] X. Cui, Atom-dimer scattering and stability of Bose and Fermi mixtures, Phys. Rev. A **90**, 041603(R) (2014).

[85] R. Zhang, W. Zhang, H. Zhai, and P. Zhang, Calibration of the interaction energy between Bose and Fermi superfluids, Phys. Rev. A **90**, 063614 (2014).

[86] M. Pierce, X. Leyronas, and F. Chevy, Few Versus Many-Body Physics of an Impurity Immersed in a Superfluid of Spin 1/2 Attractive Fermions, Phys. Rev. Lett. **123**, 080403 (2019).

[87] A. Green, J. H. S. Toh, R. Roy, M. Li, S. Kotochigova, and S. Gupta, Two-photon photoassociation spectroscopy of the $^2\Sigma^+$ YbLi molecular ground state, Phys. Rev. A **99**, 063416 (2019).

[88] A. Y. Khramov, A. H. Hansen, A. O. Jamison, W. H. Dowd, and S. Gupta, Dynamics of Feshbach molecules in an ultracold three-component mixture, Phys. Rev. A **86**, 032705 (2012).

[89] Code repository for calculating entrainment phase shift, Detecting Entrainment in Fermi-Bose Mixtures, available at https://gitlab.com/coldatoms/publications/paper_entrainment (2021).

[90] K. Hossain, S. Gupta, and M. M. Forbes, Detecting entrainment in Fermi-Bose mixtures: Code and figures, available at https://osf.io/8kc2b/ (2021).

[91] A. Bulgac, Local-density-functional theory for superfluid fermionic systems: The unitary gas, Phys. Rev. A **76**, 040502(R) (2007).

[92] F. Chevy and C. Salomon, Strongly correlated Bose gases, J. Phys. B **49**, 192001 (2016).

[93] S. Nascimbène, N. Navon, K. J. Jiang, F. Chevy, and C. Salomon, Exploring the thermodynamics of a universal Fermi gas, Nature (London) **463**, 1057 (2010).

[94] A. H. Hansen, A. Y. Khramov, W. H. Dowd, A. O. Jamison, B. Plotkin-Swing, R. J. Roy, and S. Gupta, Production of quantum-degenerate mixtures of ytterbium and lithium with controllable interspecies overlap, Phys. Rev. A **87**, 013615 (2013).

[95] K. C. Wright, R. B. Blakestad, C. J. Lobb, W. D. Phillips, and G. K. Campbell, Driving Phase Slips in a Superfluid Atom Circuit with a Rotating Weak Link, Phys. Rev. Lett. **110**, 025302 (2013).

[96] A. Ramanathan, K. C. Wright, S. R. Muniz, M. Zelan, W. T. Hill, C. J. Lobb, K. Helmerson, W. D. Phillips, and G. K. Campbell, Superflow in a Toroidal Bose-Einstein Condensate: an Atom Circuit with a Tunable Weak Link, Phys. Rev. Lett. **106**, 130401 (2011).

[97] S. Moulder, S. Beattie, R. P. Smith, N. Tammuz, and Z. Hadzibabic, Quantized supercurrent decay in an annular Bose-Einstein condensate, Phys. Rev. A **86**, 013629 (2012).

[98] A. Kumar, R. Dubessy, T. Badr, C. De Rossi, M. de Goër de Herve, L. Longchambon, and H. Perrin, Producing superfluid circulation states using phase imprinting, Phys. Rev. A **97**, 043615 (2018).

[99] M. R. Andrews, C. G. Townsend, H.-J. Miesner, D. S. Durfee, D. M. Kurn, and W. Ketterle, Observation of interference between two Bose condensates, Science **275**, 637 (1997).

[100] S. V. Iordansky, On the mutual friction between the normal and superfluid components in a rotating Bose gas, Ann. Phys. (NY) **29**, 335 (1964).

[101] Y. Cai, D. G. Allman, P. Sabharwal, and K. C. Wright, Persistent Currents in Rings of Ultracold Fermionic Atoms, Phys. Rev. Lett. **128**, 150401 (2022).

[102] M. W. Zwierlein, A. Schirotzek, C. H. Schunck, and W. Ketterle, Fermionic superfluidity with imbalanced spin populations, Science **311**, 492 (2006).

[103] Y. Takasu, K. Maki, K. Komori, T. Takano, K. Honda, M. Kumakura, T. Yabuzaki, and Y. Takahashi, Spin-Singlet Bose-Einstein Condensation of Two-Electron Atoms, Phys. Rev. Lett. **91**, 040404 (2003).

[104] A. Green, H. Li, J. H. S. Toh, X. Tang, K. C. McCormick, M. Li, E. Tiesinga, S. Kotochigova, and S. Gupta, Feshbach Resonances in *p*-Wave Three-Body Recombination within Fermi-Fermi Mixtures of Open-Shell ^{6}Li and Closed-Shell ^{173}Yb Atoms, Phys. Rev. X **10**, 031037 (2020).

[105] M. Kitagawa, K. Enomoto, K. Kasa, Y. Takahashi, R. Ciuryło, P. Naidon, and P. S. Julienne, Two-color photoassociation spectroscopy of ytterbium atoms and the precise determinations of *s*-wave scattering lengths, Phys. Rev. A **77**, 012719 (2008).

[106] B. E. Sherlock, M. Gildemeister, E. Owen, E. Nugent, and C. J. Foot, Time-averaged adiabatic ring potential for ultracold atoms, Phys. Rev. A **83**, 043408 (2011).

[107] C. Ryu, M. F. Andersen, P. Cladé, V. Natarajan, K. Helmerson, and W. D. Phillips, Observation of Persistent Flow of a Bose-Einstein Condensate in a Toroidal Trap, Phys. Rev. Lett. **99**, 260401 (2007).

[108] Y. Guo, R. Dubessy, M. de Goër de Herve, A. Kumar, T. Badr, A. Perrin, L. Longchambon, and H. Perrin, Supersonic Rotation of a Superfluid: A Long-Lived Dynamical Ring, Phys. Rev. Lett. **124**, 025301 (2020).

[109] T. van Zoest, N. Gaaloul, Y. Singh, H. Ahlers, W. Herr, S. T. Seidel, W. Ertmer, E. Rasel, M. Eckart, E. Kajari, S. Arnold, G. Nandi, W. P. Schleich, R. Walser, A. Vogel, K. Sengstock, K. Bongs, W. Lewoczko-Adamczyk, M. Schiemangk, T. Schuldt, *et al.*, Bose-Einstein condensation in microgravity, Science **328**, 1540 (2010).

[110] K. Shibata, H. Ikeda, R. Suzuki, and T. Hirano, Compensation of gravity on cold atoms by a linear optical potential, Phys. Rev. Research **2**, 013068 (2020).

[111] M. Bartenstein, A. Altmeyer, S. Riedl, R. Geursen, S. Jochim, C. Chin, J. H. Denschlag, R. Grimm, A. Simoni, E. Tiesinga, C. J. Williams, and P. S. Julienne, Precise Determination of ^{6}Li Cold Collision Parameters by Radio-Frequency Spectroscopy on Weakly Bound Molecules, Phys. Rev. Lett. **94**, 103201 (2005).